Bull Volcanol (2010) 72:657–669
DOI 10.1007/s00445-010-0349-8

RESEARCH ARTICLE

# Precursory activity of the 161 ka Kos Plateau Tuff eruption, Aegean Sea (Greece)

**David J. W. Piper · Georgia Pe-Piper · Darren Lefort**

Received: 16 October 2008 / Accepted: 20 January 2010 / Published online: 25 February 2010


**Abstract** The Kos Plateau Tuff (KPT) eruption of 161 ka was the largest explosive Quaternary eruption in the eastern Mediterranean. We have discovered an uplifted beach deposit of abraded pumice cobbles, directly overlain by the KPT. The pumice cobbles resemble pumice from the KPT in petrography and composition and differ from Plio-Pleistocene rhyolites on the nearby Kefalos Peninsula. The pumice contains enclaves of basaltic andesite showing chilled lobate margins, suggesting co-existence of two magmas. The deposit provides evidence that the precursory phase of the KPT eruption produced pumice rafts, and defines the paleoshoreline for the KPT, which elsewhere was deposited on land. The beach deposit has been uplifted about 120 m since the KPT eruption, whereas the present marine area south of Kos has subsided several hundred metres, as a result of regional neotectonics. The basaltic andesite is more primitive than other mafic rocks known from the Kos–Nisyros volcanic centre and contains phenocrysts of $Fo_{89}$ olivine, bytownite, enstatite and diopside. Groundmass amphibole suggests availability of water in the final stages of magma evolution. Geochemical and mineralogical variation in the mafic products of the KPT eruption indicate that fractionation of basaltic magma in a base-of-crust magma chamber was followed by mixing with rhyolitic magma during eruption. Low eruption rates during the precursory activity may have minimised the extent of mixing and preserved the end-member magma types.

**Keywords** Kos Plateau Tuff · Basaltic andesite · Neotectonics · Beach · Conglomerate · Rhyolite · Precursory eruption

Editorial responsibility: J. McPhie

**Electronic supplementary material** The online version of this article (doi:10.1007/s00445-010-0349-8) contains supplementary material, which is available to authorized users.

D. J. W. Piper (✉)
Geological Survey of Canada (Atlantic),
Bedford Institute of Oceanography,
P.O. Box 1006, Dartmouth, Nova Scotia B2Y 4A2, Canada
e-mail: dpiper@nrcan.gc.ca

G. Pe-Piper · D. Lefort
Department of Geology, Saint Mary's University,
Halifax, Nova Scotia B3H 3C3, Canada

## Introduction

### Setting and purpose

The islands of Kos and Nisyros form the most easterly volcanic centre of the South Aegean volcanic arc (Pe-Piper and Piper 2005). The Kos Plateau Tuff (KPT) eruption at 161 ka was the largest Quaternary eruption in the eastern Mediterranean (Allen 2001). Remnants of a pre-KPT stratovolcano are preserved as subaerial dacites on the islets of Pachia and Pyrgousa and as submarine volcanic rocks on Nisyros. Predominantly subaerial volcanic rocks on Nisyros and the islets of Pyrgousa, Yali and Strongili postdate the KPT.

We have serendipitously discovered a previously unknown conglomerate immediately below the KPT, at Akra Chelona in southern Kos (Fig. 1b). The deposit consists of rounded cobbles of rhyolitic pumice that contain decimetre-sized basaltic andesite enclaves, together with basaltic andesite pebbles, forming a 1-m-thick conglomerate. The objectives of this paper are to use this deposit to understand the precursory phase of eruption of the KPT and the paleogeographic setting leading up to the KPT eruption. Although mafic magma has been inferred to have triggered

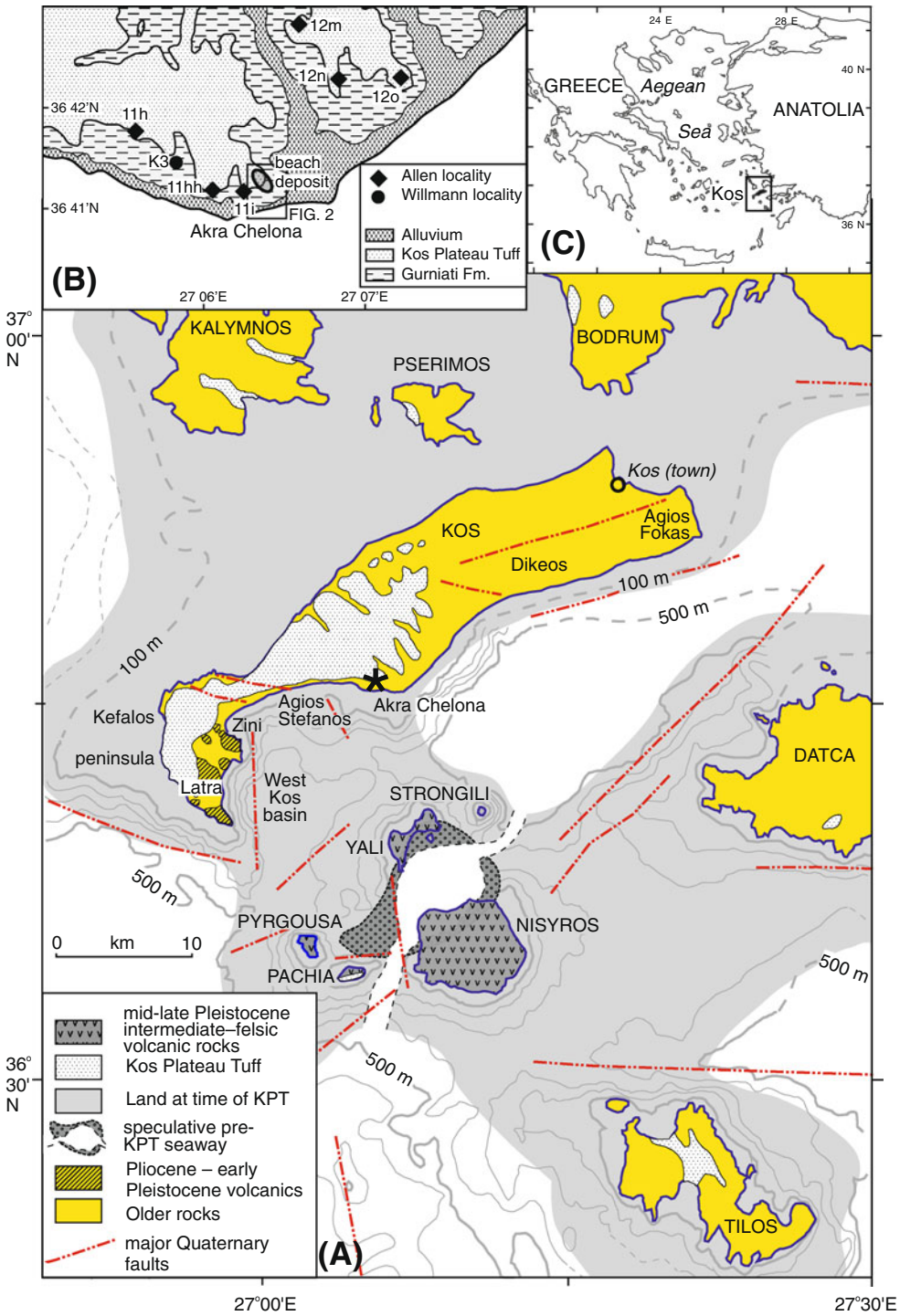


**Fig. 1** **a** Map of Kos, Nisyros and adjacent islands showing the distribution of the Kos Plateau Tuff (modified from Allen et al. 1999; Pe-Piper et al. 2005). **b** Detail of study location and nearby sections of Willmann (1983) and Allen et al. (1999). **c** Location of Kos in the Aegean Sea

the KPT eruption (e.g. Bachmann et al. 2007), it has previously been known only from andesitic pumice (Allen 2001), so a third objective is to use the petrology and geochemistry of the basaltic andesite enclaves to better understand the petrogenesis of the KPT magmas. A fourth objective is to use the paleoshoreline defined by the conglomerate to further constrain the rates and style of neotectonic deformation in the area.

This study thus contributes to the more general issues of the triggering and character of large explosive eruptions in volcanoes at or near sea level. A precursory phreatic or phreatomagmatic stage has been identified in the 1883 Krakatau eruption (Simkin and Fiske, 1983) and the Minoan eruption of Santorini (Heiken and McCoy 1990). Defining the style of precursory activity in the KPT eruption thus broadens our understanding of such precur-

sory eruptions. The injection of mafic magma into a felsic magma chamber has been widely proposed as the trigger for explosive silicic eruptions (e.g. Murphy et al. 2000; Shane et al. 2005), but the temporal evolution of such mafic magma is poorly understood. It is commonly highly mixed with the dominant rhyolitic eruptive products by shear in the vent. Its preservation in the Akra Chelona conglomerate provides an opportunity to assess the evolution of such mafic triggers.

### The Kos Plateau Tuff eruption

Six major stratigraphic units have been identified in the KPT (Allen et al. 1999). Unit A, at the base, is a <1.5-m-thick ash-fall layer, thicker to the southeast of the vent and only 10–30 mm thick on Kos. Units B, C and the lower part of F are internally stratified pyroclastic flow deposits and units D and E are a series of massive ignimbrites, with total thicknesses exceeding 17 m on southern Kos. The top of unit F is a >1-m-thick vitric ash-fall bed. The base of unit E is the coarsest pyroclastic deposit; lithic clasts 0.1–0.3 m in size are common. The KPT consists principally of rhyolitic ash and pumice, with minor andesitic pumice (58–63 wt.% $SiO_2$) and lithic clasts of andesite, dacite and metamorphic basement rocks. The volcanic lithic clasts appear to be derived from an older stratocone, remnants of which are exposed on the islets of Pyrgousa and Pachia (Fig. 1a). Based on the estimate of >60 $km^3$ (DRE) of erupted volume and the stratigraphy of the KPT, Allen (2001) proposed a ~20-km-wide caldera, centred on the present young volcanic island of Yali. In contrast, based on seismic reflection profiles, Pe-Piper et al. (2005) interpreted the source of the KPT to lie between Yali and Nisyros, where it is now obscured by the younger volcanic rocks of Nisyros, Yali and Strongili (Fig. 1a).

From their detailed study of the KPT, Allen and Cas (2001) proposed that the pyroclastic flows travelled tens of kilometres across the sea. This interpretation was challenged by Pe-Piper et al. (2005), who showed on the basis of seismic reflection profiles that much of the area around the proposed vent was land at the time of the eruption and has since subsided. The shoreline northeast of the eruptive centre was interpreted to extend from Akra Chelona in southern Kos to just north of Strongili.

## Methods

Samples of cobbles and pebbles were chipped, washed and crushed using a shatterbox with an iron bowl. Major and trace elements were determined by methods described by Activation Laboratories Ltd. (2006) using their Code 4Lithoresearch and Code 4B1 packages, which combine lithium metaborate/tetraborate fusion ICP whole rock analysis with a trace element ICP-MS package. Detection limits are shown in Table 1. Nd isotopes were determined using methods summarised by Pe-Piper and Moulton (2008).

Mineral chemistry was determined from polished thin sections using a JEOL-733 electron microprobe equipped with four wavelength spectrometers and a Tracor Northern 145-eV energy dispersive detector. The instrument was operated at 15 kV with a 15 nA beam current and a beam diameter of ~3 μm. Calibration used geological standards and specific reference minerals, and the data were reduced using a Tracor Northern ZAF matrix-correction programme. Backscattered electron images were taken to characterise compositional zoning and growth patterns and porosity in pumice was determined by image analysis of these images. Pumice density was determined from measured weight and volume.

## Results

### Field observations

The observations were made near the top of section K3 of Willmann (1983), 2 km west of localities 12o and 12n and 0.5 km east of locality 11h of Allen et al. (1999), at 36°45.549′N 27°06.337′E and an elevation of 49 m (Fig. 1b). Outcrop is discontinuous in natural cliffs cut by deeply incised ephemeral streams and largely obscured by vegetation and thin soil. Regionally, black shales and minor sandstones of the Upper Pliocene fluvial and lacustrine Gurniati Formation (Willmann 1983) dip 15° to the north and are unconformably overlain by the flat-lying KPT. At the new locality, immediately overlying the unconformity and below the main KPT succession, is a 1-m-thick conglomerate that is well exposed as a result of cutting of an unpaved road up the hillside (Fig. 2).

The clasts in the conglomerate are almost exclusively cobbles (64–256 mm) and pebbles (4–64 mm) of rhyolitic pumice and basaltic andesite; one small chert pebble was found. The upper part of the conglomerate has an openwork structure that is partly infiltrated by the overlying KPT (Fig. 2c). The lower part of the conglomerate has a sandy matrix. Matrix components are similar to those in the clasts and the conglomerate is in places matrix supported (Fig. 2a, c). Despite this sandy matrix, nowhere was well-sorted sand with sedimentary structures seen. Neither was any large bioclast seen. In the lower part of the conglomerate, clasts are predominantly spherical basaltic andesite pebbles. The middle part of the conglomerate consists predominantly of flat basaltic andesite pebbles, and the upper part of the conglomerate consists of rhyolite pumice

**Table 1** Geochemical analyses of clasts

| | Detection limit | Basaltic andesite | | Rhyolitic pumice | |
|---|---|---|---|---|---|
| | | CS166 | CS167 | CS168F | CS169F |
| Major elements in wt.% | | | | | |
| $SiO_2$ | 0.01 | 54.45 | 52.31 | 72.1 | 69.73 |
| $TiO_2$ | 0.001 | 0.72 | 0.77 | 0.25 | 0.25 |
| $Al_2O_3$ | 0.01 | 16.37 | 16.52 | 12.85 | 13.79 |
| $Fe_2O_3T$ | 0.01 | 6.11 | 6.5 | 1.91 | 1.89 |
| MnO | 0.001 | 0.119 | 0.125 | 0.060 | 0.060 |
| MgO | 0.01 | 5.75 | 6.37 | 0.44 | 0.37 |
| CaO | 0.01 | 10.06 | 10.9 | 1.42 | 1.41 |
| $Na_2O$ | 0.01 | 3.00 | 2.86 | 3.91 | 4.04 |
| $K_2O$ | 0.01 | 1.25 | 1.00 | 3.81 | 3.86 |
| $P_2O_5$ | 0.01 | 0.13 | 0.13 | 0.05 | 0.05 |
| LOI | | 0.71 | 0.96 | 3.76 | 3.56 |
| Total | 0.01 | 98.69 | 98.44 | 100.6 | 99.01 |
| Trace elements in ppm | | | | | |
| Sc | 1 | 25 | 27 | 2 | 2 |
| Be | 1 | 2 | 2 | 2 | 2 |
| V | 5 | 180 | 195 | 17 | 15 |
| Cr | 20 | 170 | 180 | 30 | 40 |
| Co | 1 | 23 | 26 | 2 | 2 |
| Ni | 1 | 66 | 72 | 17 | 15 |
| Cu | 1 | 28 | 28 | 4 | 23 |
| Zn | 1 | 65 | 56 | 36 | 33 |
| Cd | 0.5 | <0.5 | <0.5 | <0.5 | <0.5 |
| S | 0.001 | 0.03 | 0.02 | 0 | 0 |
| Ga | 1 | 17 | 17 | 18 | 17 |
| Ge | 0.5 | 1.2 | 1.3 | 1.2 | 1.2 |
| As | 5 | <5 | <5 | 5 | 9 |
| Rb | 1 | 29 | 25 | 107 | 105 |
| Sr | 2 | 368 | 386 | 173 | 175 |
| Y | 0.5 | 18.4 | 19.2 | 14.7 | 14.2 |
| Zr | 1 | 98 | 91 | 189 | 172 |
| Nb | 0.2 | 8.1 | 7.7 | 22.9 | 22.6 |
| Mo | 2 | <2 | <2 | 3 | 4 |
| Ag | 0.3 | 0.5 | 0.9 | 0.6 | 0.6 |
| In | 0.1 | <0.1 | <0.1 | <0.1 | <0.1 |
| Sn | 1 | 1 | 1 | 2 | 5 |
| Sb | 0.2 | 2.7 | 3.4 | <0.2 | <0.2 |
| Cs | 0.1 | 0.9 | 0.8 | 3.3 | 3.2 |
| Ba | 3 | 330 | 274 | 911 | 918 |
| La | 0.05 | 16.3 | 14.2 | 34.9 | 34.7 |
| Ce | 0.05 | 31.5 | 28.4 | 59.2 | 57.6 |
| Pr | 0.01 | 3.17 | 2.94 | 5.02 | 5.00 |
| Nd | 0.05 | 13.1 | 12.5 | 14.5 | 14.9 |
| Sm | 0.01 | 3.01 | 2.97 | 2.50 | 2.53 |
| Eu | 0.005 | 1 | 1.03 | 0.51 | 0.52 |
| Gd | 0.01 | 3.14 | 3.02 | 2.11 | 2.09 |
| Tb | 0.01 | 0.52 | 0.53 | 0.35 | 0.33 |

**Table 1** (continued)

| | Detection limit | Basaltic andesite | | Rhyolitic pumice | |
|---|---|---|---|---|---|
| | | CS166 | CS167 | CS168F | CS169F |
| Dy | 0.01 | 3.18 | 3.22 | 2.09 | 1.98 |
| Ho | 0.01 | 0.65 | 0.66 | 0.45 | 0.43 |
| Er | 0.01 | 1.99 | 1.91 | 1.44 | 1.39 |
| Tm | 0.005 | 0.3 | 0.29 | 0.24 | 0.23 |
| Yb | 0.01 | 1.93 | 1.86 | 1.64 | 1.58 |
| Lu | 0.002 | 0.31 | 0.29 | 0.26 | 0.26 |
| Hf | 0.1 | 2.6 | 2.4 | 4.6 | 4.2 |
| Ta | 0.01 | 0.73 | 0.62 | 1.60 | 1.59 |
| W | 0.5 | 0.5 | 0.7 | <0.5 | <0.5 |
| Tl | 0.05 | 0.14 | 0.13 | 0.32 | 0.33 |
| Pb | 3 | <3 | <3 | 11 | 8 |
| Bi | 0.1 | <0.1 | 0.1 | 0.2 | 0.2 |
| Th | 0.05 | 4.08 | 3.19 | 14.4 | 14.2 |
| U | 0.01 | 1.23 | 0.95 | 4.25 | 4.15 |
| $\varepsilon_{Nd}$ | | n.d. | 1.7 | n.d. | −0.3 |

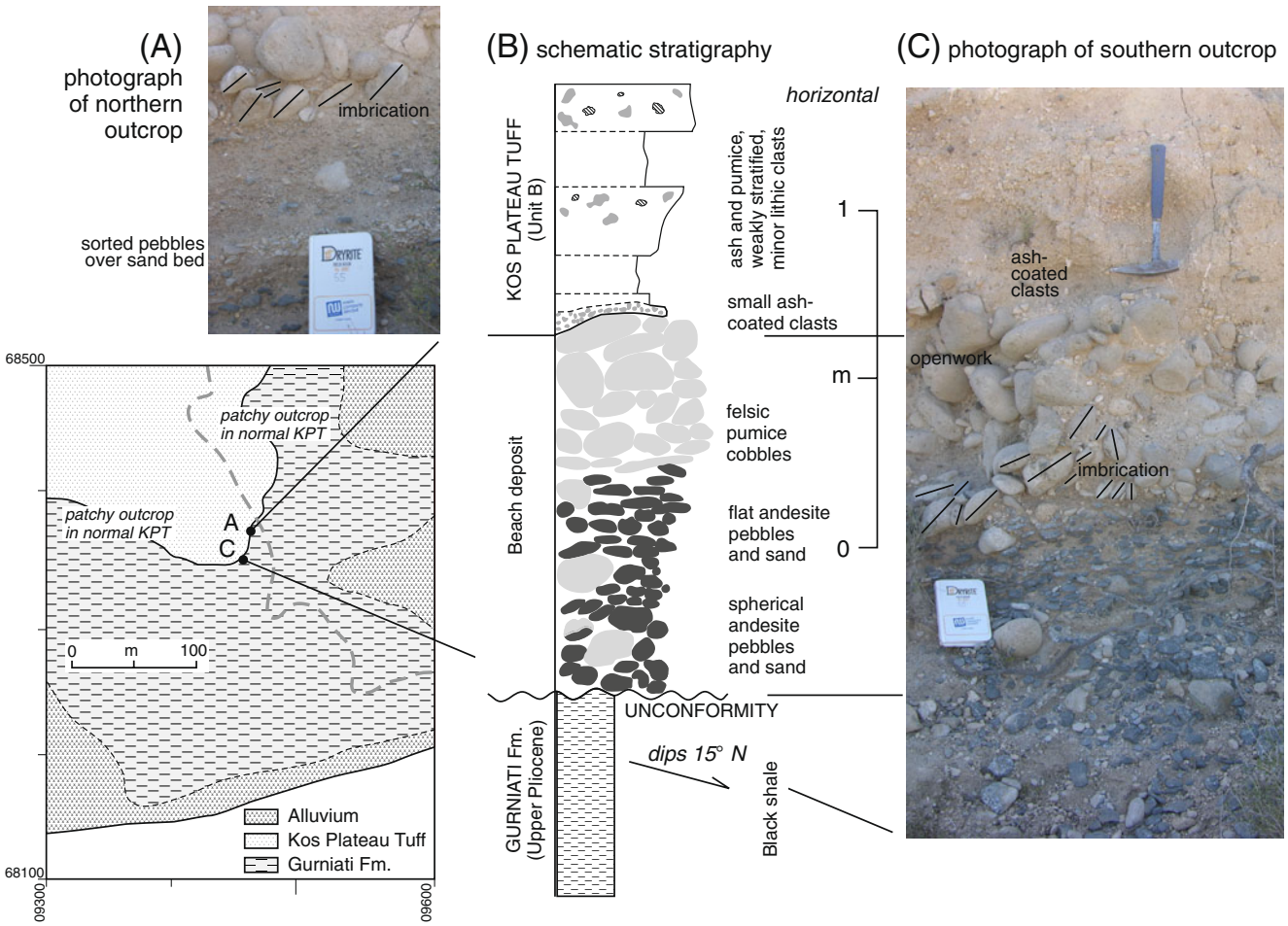


**Fig. 2** Detailed map showing location of Akra Chelona conglomerate, with photographs showing sections through the northern (**a**) and southern (**c**) parts of the conglomerate. **b** is a schematic stratigraphic section

cobbles (Fig. 2b, c). Rare pumice pebbles and cobbles and abundant pumiceous sand are found in the lower basaltic andesite-dominated conglomerate. Some of the pumice cobbles contain rounded enclaves (up to a dm in size) of basaltic andesite (Fig. 3). The size of the largest enclaves is comparable with the largest basaltic andesite pebbles, some of which preserve remnants of pumice in surface depressions. Locally, a bed of well-sorted pebbles directly overlies a thin bed of sand, with no evidence of an erosional base (Fig. 2a). South-dipping imbrication is common in pebbles and cobbles (Fig. 2a, c).

Although outcrop is discontinuous, it appears that the unconformity at the top of the Gurniati Formation is generally planar: there is no evidence that the cobble conglomerate occupies a channel. The conglomerate appears to thin out to the north and west over a distance of tens of metres. To the southeast, the conglomerate is truncated by recent erosion (Fig. 2).

No evidence was found for unit A of the KPT, which ranges in thickness from 20–33 mm in six outcrops within 2 km of the Akra Chelona conglomerate (Allen 1998, Fig. 5.2; Allen et al. 1999). The conglomerate appears to be directly overlain by unit B of the KPT, a weakly stratified pumice lapilli and ash layer with a few lithic clasts; unit B has infiltrated between the cobbles. There is no evidence of weathering or a paleosol at the contact. Centimetre-size clasts thickly coated with ash are locally common at the base of the KPT unit (Fig. 2b, c) and have been noted elsewhere in unit B (Allen et al. 1999).

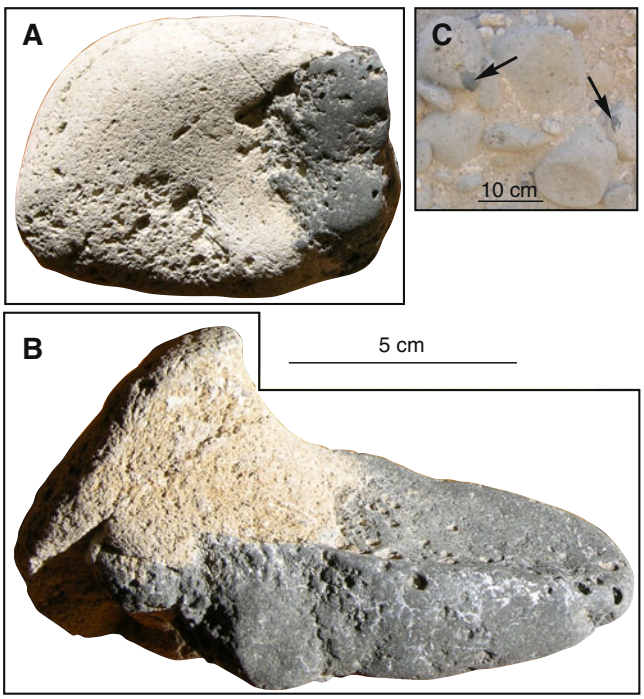


**Fig. 3** Photographs of cobbles of mingled rhyolite pumice and basaltic andesite. **a**, **b** Pumice cobbles with large basaltic andesite enclaves; **c** outcrop showing pumice cobbles with small parts of basaltic andesite enclaves exposed (indicated by *arrows*)

## Lithogeochemistry

Whole rock geochemical analyses were made of two representative samples of each of the dominant lithologies in the conglomerate: basaltic andesite pebbles and rhyolite pumice cobbles. These analyses show that the pebbles are basaltic andesite in the IUGS classification (Fig. 4). They have high MgO (~6 wt.%) and Cr (~175 ppm) contents (Fig. 5). Rare-earth elements show slight light REE enrichment (Fig. 6). The pumice cobbles are of rhyolite composition (Figs. 4 and 5) with a fractionated REE pattern including a negative Eu anomaly (Fig. 6). Nd isotopes were determined on one pumice and one basaltic andesite (Table 1), giving values of $\varepsilon_{Nd}$=+1.7 for the basaltic andesite and $\varepsilon_{Nd}$=−0.3 for the rhyolitic pumice.

## Petrography and mineral chemistry

### Basaltic andesite

Basaltic andesite is found as pebbles in the Akra Chelona conglomerate and as pebble-sized enclaves within the pumice clasts (Fig. 3). It contains phenocrysts and glomerocrysts (~15–25 modal % of rock) of plagioclase (~55 modal % of phenocrysts), clinopyroxene (~40 modal %), olivine (~2 modal %) and orthopyroxene (0–3 modal %), together with microphenocrysts (~10–15 modal %) of these minerals plus pyrrhotite and hornblende (Fig. 7a). The groundmass (~55 modal %) is pilotaxitic subophitic, consisting of equigranular plagioclase, hornblende and interstitial glass, with 10–15% porosity. Some vesicles are ovoid, but many are angular with margins defined by phenocrysts and show no systematic elongation (Fig. 7c).

Many plagioclase phenocrysts show compositional zoning and spongy cellular (sieve) texture. Two types of spongy cellular texture are present: (1) a spongy cellular core is surrounded by a rim of clear plagioclase (1 in Fig. 7a) and (2) a clear core is surrounded by a rim of spongy texture, then a clear rim of plagioclase. Plagioclase also has “straw” texture in some laths. Inclusions found in plagioclase include clinopyroxene and pyrrhotite. The most mafic basaltic andesite (CS167) has the most anorthitic feldspar (bytownite, $An_{82}$ to $An_{87}$, calcic cores) and the most magnesian olivine ($Fo_{84}$ to $Fo_{89}$, magnesian cores) and pyroxenes (Fig. 8). Other basaltic andesite samples have a similar dominant composition of phenocrysts, but include some less calcic plagioclase and less magnesian olivine. Clinopyroxenes are augite, endiopside or diopside and have cores with up to 6.6 wt.% $Al_2O_3$ and generally show reverse zoning (more Fe-rich cores; Fig. 9b). Some

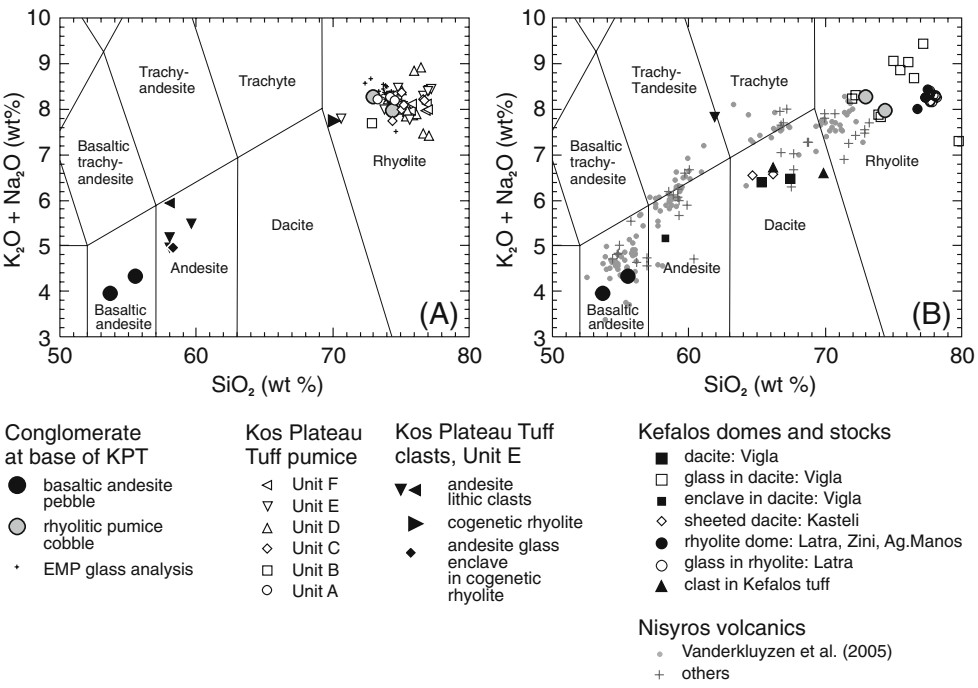


**Fig. 4** IUGS classification of cobbles and pebbles from the Akra Chelona conglomerate, showing their comparison with other rocks. **a** Compared with pumice and lithic clasts from the KPT (data principally from Allen 1998; lithic clasts and some unit E pumice from Pe-Piper and Moulton 2008). **b** Compared with Pliocene to Lower Pleistocene domes and stocks of the Kefalos Peninsula (from Pe-Piper and Moulton 2008), volcanic rocks of Nisyros (from Vanderkluysen et al., 2005 and several older sources summarised by Pe-Piper and Piper 2002, their Fig. 275)

clinopyroxene phenocrysts show sector zoning. Pyrrhotite occurs as tiny inclusions within some clinopyroxene phenocrysts. The minor orthopyroxene is enstatite ($En_{60–65}$: Fig. 8c); some enstatite phenocrysts are entirely engulfed by clinopyroxene and the accessory mineral apatite is found along the rim (Fig. 9a). The groundmass amphiboles (Fig. 9b) are predominantly magnesio-hastingsite and magnesio-hornblende with a few ranging into the tschermakite field (Fig. 8d). The $Al_2O_3$ content of the amphiboles reaches up to 14 wt.%. Ti-magnetite (~10 wt.% $TiO_2$) and pyrrhotite are widespread in the groundmass.

Basaltic andesite is also found as millimetre- to centimetre-size enclaves in thin sections of rhyolitic pumice. Some enclaves show lobate texture, indicative of co-existence of two immiscible liquids with different surface tension, and all show a finer grained outer margin that is evidence of chilling (Fig. 7b). The enclaves compare texturally to the basaltic andesite pebbles but lack vesicles and have no glass in the groundmass.

## Rhyolite pumice

The rhyolite pumice is slightly porphyritic. It contains millimetre-size phenocrysts (~3 modal %) of plagioclase (65–80 modal % of phenocrysts), quartz, sanidine and orthopyroxene in decreasing order of abundance, set in a hyalopilitic groundmass of glass with microphenocrysts of sanidine, quartz, Ti-magnetite, hornblende and apatite and a few plagioclase microlites (Fig. 7e). Some plagioclase phenocrysts show twinning and compositional zoning. Plagioclase phenocrysts have a compositional range of $An_{36}$–$An_{44}$, most commonly with Ca-rich rims. The groundmass ranges from predominantly colourless to

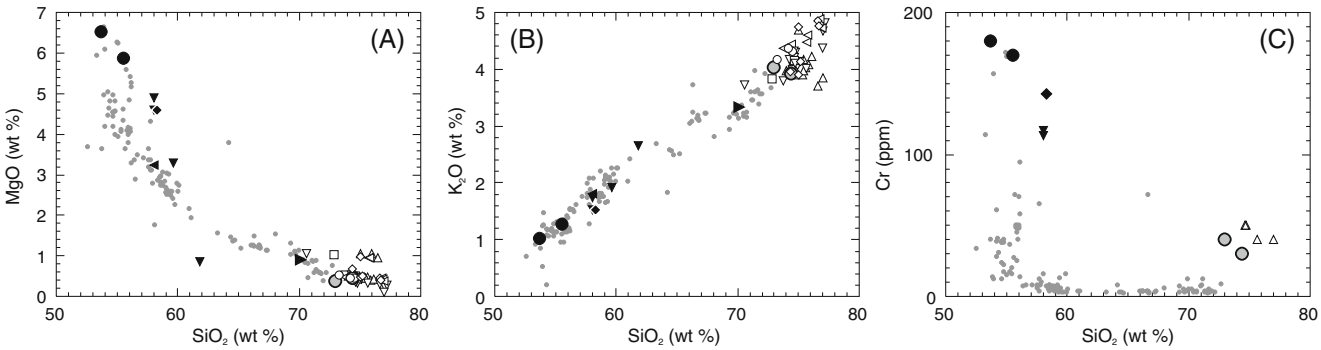


**Fig. 5** **a**–**c** Plots of MgO, $K_2O$ and Cr against $SiO_2$ for the cobbles and pebbles from the Akra Chelona conglomerate, compared with pumice and lithic clasts from the Kos Plateau Tuff (from Allen 1998 and Pe-Piper and Moulton 2008) and volcanic rocks of Nisyros (from Vanderkluysen et al. 2005). Symbols as in Fig. 4

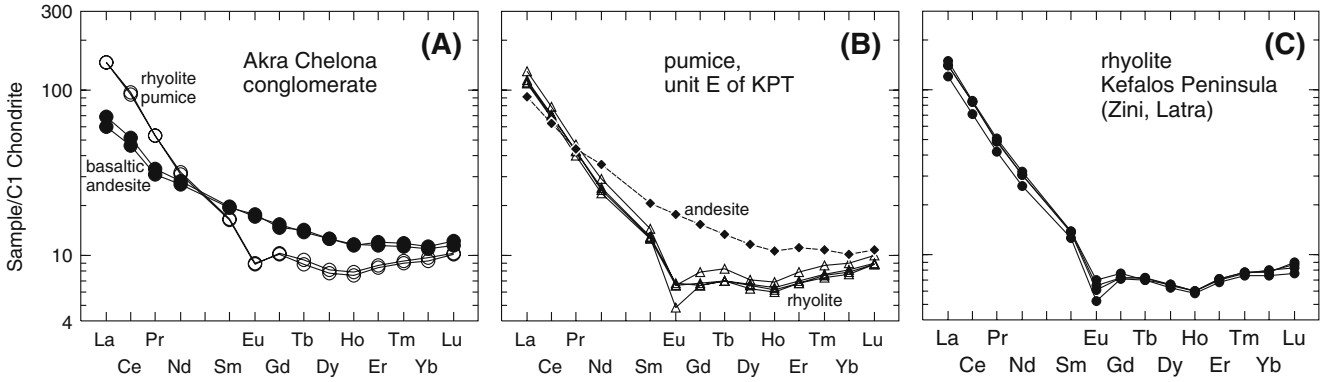


**Fig. 6** REE plots for (**a**) the cobbles and pebbles from the Akra Chelona conglomerate, compared with those for (**b**) lithic clasts and pumice from unit E of the KPT and (**c**) Pliocene and Early Pleistocene rhyolite, Kefalos Peninsula. Data for **b** and **c** from Pe-Piper and Moulton (2008). Symbols as in Fig. 4

brown glass to predominantly spherulitic and some domains consist of a glass–spherulite combination (Fig. 7d). The glass compositions determined with a defocussed beam by electron microprobe are similar to bulk rhyolite compositions (Fig. 4). In the most porous parts of the pumice, vesicles are ovoid to irregular, in places little deformed and in places sheared to aspect ratios as great as 7:1 (Fig. 7d). They most closely resemble the

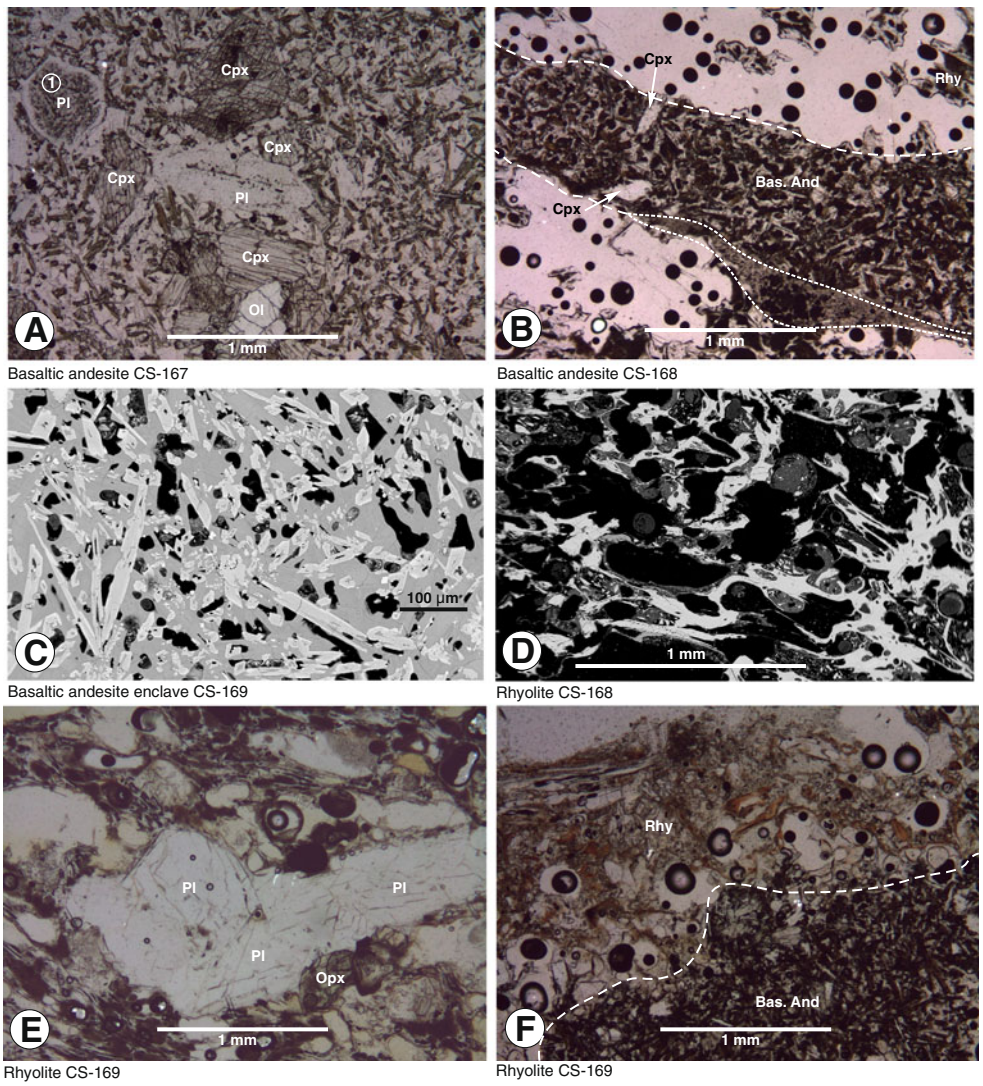


**Fig. 7** Textural and mineralogical features of the cobbles and pebbles from the Akra Chelona conglomerate. **a** Microphotograph of basaltic andesite with plagioclase (*Pl*), clinopyroxene (*Cpx*), olivine (*Ol*) phenocrysts in a groundmass of hornblende, plagioclase and glass. (*1*) is plagioclase phenocryst with sieve textured core and clear rim. **b** Microphotograph of a basaltic andesite enclave (*Bas. And*) in a glassy rhyolite host (*Rhy*) with lobate texture (*dashed red line*) and chilled margin (*dotted yellow line*). The enclave has clinopyroxene and plagioclase phenocrysts in a groundmass of hornblende and plagioclase. **c** Backscattered electron image showing character of vesicles (*black*) in basaltic andesite. **d** Backscattered electron image showing character of vesicles (*black*) in a more porous example of rhyolite. **e** Microphotograph of rhyolitic pumice with a large plagioclase and orthopyroxene glomerocryst. Groundmass consists of clear to brown glass and very few phenocrysts. **f** Microphotograph of contact of rhyolite enclave (*dashed red line*) with basaltic andesite host

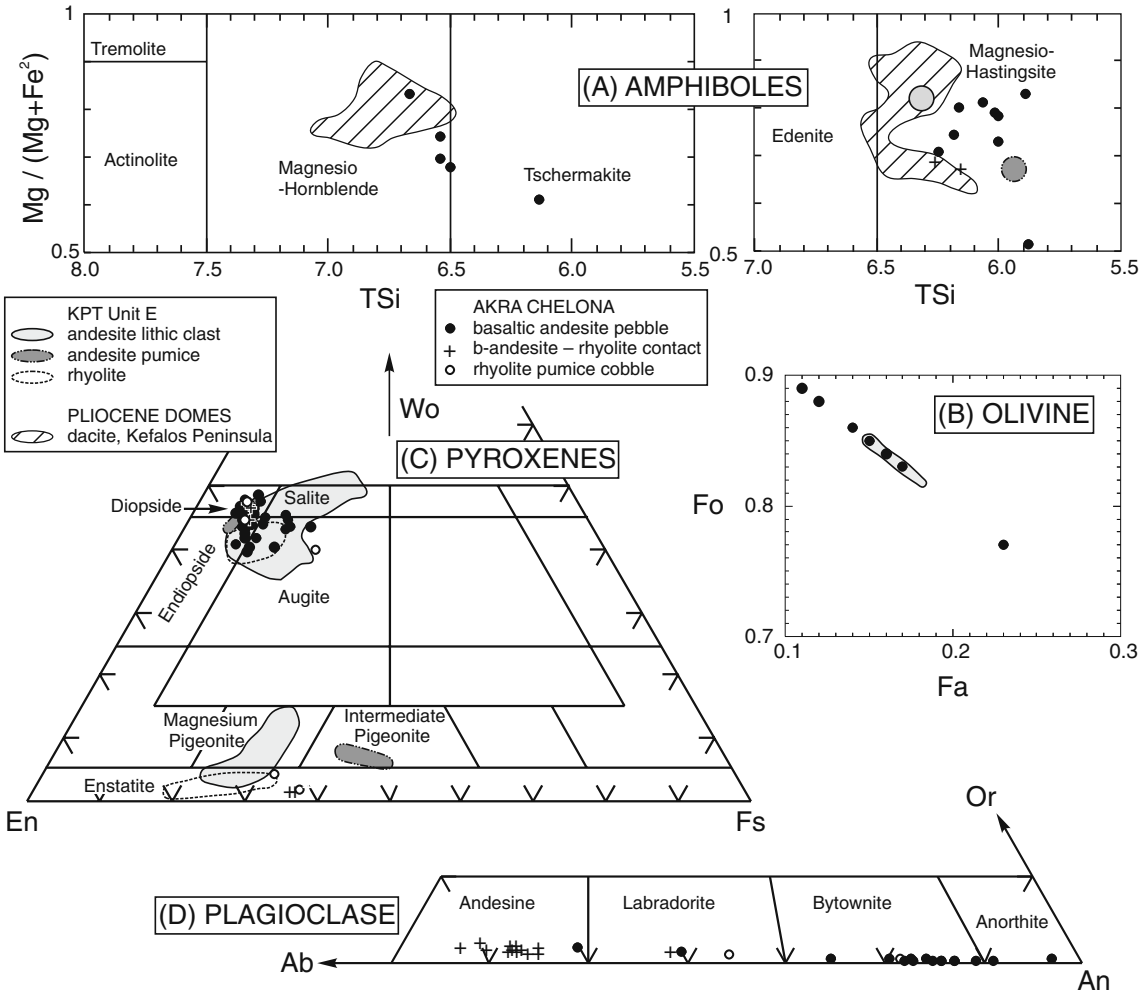


**Fig. 8** Diagrams summarising composition of phenocrysts in the basaltic andesite pebbles and comparison with those in andesite lithic clasts from unit E of the KPT. **a** Amphibole, **b** olivine, **c** pyroxene, **d** plagioclase. Data for unit E of the KPT and the Kefalos Peninsula from Pe-Piper and Moulton (2008)

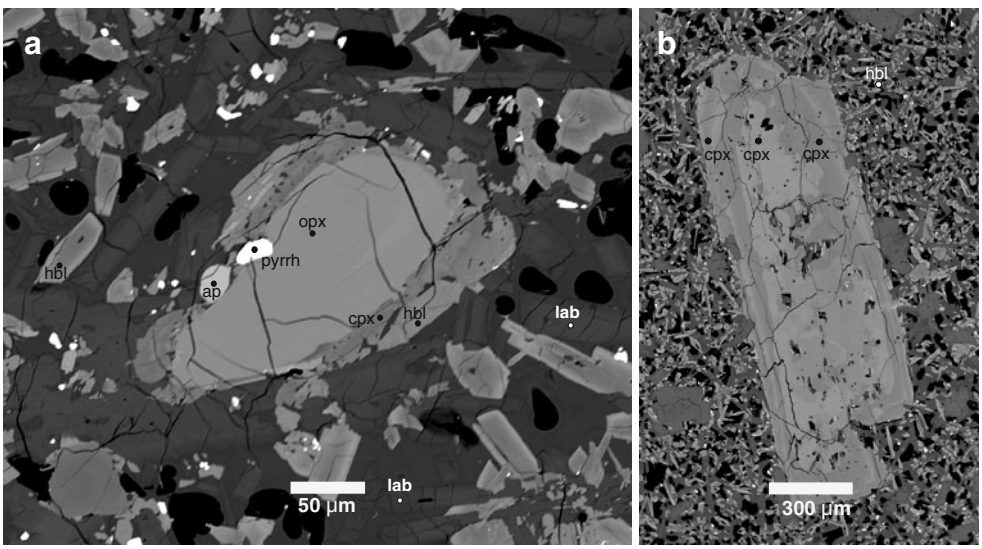


Basaltic andesite CS-168

**Fig. 9** Backscattered electron images of pyroxene phenocrysts in basaltic andesite. **a** Orthopyroxene rimmed by small apatite and pyrrhotite and mantled by clinopyroxene and then hornblende. **b** Zoned clinopyroxene

frothy vesicular rhyolite from the KPT (Bouvet de Maisonneuve et al. 2009) except that the vesicles are not as large. The proportion of vesicles determined on 2-D thin-section images ranges from 35–70 modal % in different parts of the pumice. The density of the pumice is 780 kg $m^{-3}$.

Rhyolitic enclaves are found in one basaltic andesite sample (CS169). The contact is lobate, but shows no chilling (Fig. 7f). The rhyolite is similar to the main vesicular pumice in petrography and composition of the glass.

## Discussion

### The geochemical and petrographic affinity of the pebbles and cobbles

Of the >150 geochemical analyses in the literature of the post-KPT volcanic rocks from Nisyros, only one is as primitive (on the basis of MgO, Cr and $SiO_2$ content) as basaltic andesite CS167 from this study (Fig. 5). This sample, AV24b, is from a lithic clast in the Stavros pyroclastic flow and surge deposits of basaltic to andesitic composition (Vanderkluysen et al. 2005). The main cluster of basaltic andesite analyses from Nisyros (Fig. 4) is more evolved, having higher $Na_2O$ (3.1–3.5 wt.%) and lower MgO (4–5 wt.%) and Cr (<70 ppm; Fig. 5) than the most evolved basaltic andesite (CS166) from this study.

The KPT contains lithic clasts of andesite, eroded from older lavas adjacent to vents and pumiceous andesite glass (Fig. 4; Allen 1998). This andesite glass has higher MgO and Cr than do lavas from Nisyros with the same $SiO_2$ content (Fig. 5). LREE are more fractionated than in the basaltic andesite pebbles. Lithic clasts of andesite from the KPT have $\varepsilon_{Nd}$=+0.2 (Pe-Piper and Moulton 2008), compared with a more primitive $\varepsilon_{Nd}$=+1.7 for the basaltic andesite pebble.

Bulk chemical composition of the rhyolite pumice cobbles is similar in major element composition (Figs. 4 and 5) to pumice from unit A and to some analyses from unit B of the KPT reported by Allen (1998). Higher units in the KPT are a little more siliceous and unit E has greater REE fractionation. Pumice from unit E has $\varepsilon_{Nd}$=+0.6–+1.1 and from unit B +0.2–+0.5 (Bachmann et al. 2007), compared with $\varepsilon_{Nd}$=–0.3 for the rhyolitic pumice cobbles.

Plio-Pleistocene rhyolite domes of the Kefalos Peninsula (Fig. 1a) differ from the pumice cobbles in being higher in silica and alkalis (Fig. 4; Pe-Piper and Moulton 2008). The pumice cobbles show less Eu fractionation than either the Kefalos Peninsula rhyolites or pumice from unit E of the KPT (Fig. 6). The Kefalos Peninsula rhyolites have strikingly lower Zr (~77 ppm cf. ~180 ppm in the cobbles) and Nb (~16 ppm cf. ~23 ppm), but most other trace element abundances are similar in the pumice cobbles and the Kefalos Peninsula rhyolites.

Petrographically, the small plagioclase, quartz and sanidine phenocrysts in the pumice cobbles are similar in relative abundance and size to those in the KPT pumice (e.g. Stadlbauer 1988 and our own data), although orthopyroxene appears more abundant and biotite less abundant than in the KPT. Phenocrysts are smaller and less abundant than those in the Kefalos tuff (Allen et al. 2009).

In summary, basaltic andesite does not outcrop anywhere on Kos and none is known as clasts in the KPT. A similar basaltic andesite is known as a clast in a post-KPT pyroclastic unit on Nisyros. Pumice from unit A of the KPT is the closest geochemical and petrographic match for the rhyolitic pumice cobbles. The $\varepsilon_{Nd}$ in the cobbles is a little lower than in the KPT, and in the KPT $\varepsilon_{Nd}$ values increase at stratigraphically higher levels (Bachmann et al. 2007).

### The age of the Akra Chelona conglomerate

Stratigraphic evidence suggests that the Akra Chelona conglomerate was associated with a precursory stage of the KPT eruption. There is no evidence for weathering or a paleosol at the top of the conglomerate. The conglomerate is directly overlain by the first pyroclastic flow unit, B, of the KPT, which percolated into the interstices of the conglomerate.

### The depositional environment of the conglomerate

Several observations suggest that the Akra Chelona conglomerate is a beach deposit. Despite the coarse-grained character of the conglomerate, it does not appear to occupy a channel, but rather thins out gradually northward and westward to where the base of the KPT is marked by the unconformity with a paleosol (Allen et al. 1999). Openwork conglomerates are found in several environments, including beaches. The concentration of flat pebbles is very characteristic for the upper part of a beach (e.g. Bluck 1999), which in this case may have prograded over more spherical pebbles on the lower part of the beach (Fig. 2b, c). The presence of well-sorted pebbles directly over a thin sand bed (Fig. 2a) is common on beaches, but rare in rivers (e.g. Bluck 1999). The internal organisation of the conglomerate suggests that was not a tsunami deposit (cf. Fujino et al. 2006, Morton et al. 2007) and we argue below that the presence of basaltic andesite pebbles would require prolonged beach reworking.

Beach deposits are rarely preserved in the geological record: the preservation of the Akra Chelona beach was probably a consequence of its rapid burial by the overlying

KPT. Unit A of the KPT, interpreted as phreatoplinian ash, is absent at the Akra Chelona locality, but 20–30 mm thick at nearby localities where the KPT rests unconformably on the weathered surface of the Gurniati Formation (Allen et al. 1999). This distribution is to be expected: ash would accumulate on land, but would be reworked on a beach.

## Paleogeographic and volcanologic implications of the Akra Chelona beach conglomerate

The Akra Chelona beach conglomerate consists almost entirely of volcanic products. The basaltic andesite pebbles are identical to the basaltic andesite enclaves in the pumice, suggesting that the pebbles were liberated from the pumice by abrasion on the beach. The coarse enclave-bearing pumice clasts were probably part of pumice rafts that got stranded, thus accounting for the absence of other clast types on the beach. Abrasion and destruction of pumice on beaches may take weeks to months (e.g. Bryan et al. 2004).

Abrasion has destroyed any external surface textures on the pumice clasts and has selectively preserved the more robust lithologies. The largest pumice cobbles are less than 15 cm mean diameter; pumice clasts of this size are sufficient to float the largest observed basaltic andesite pebble. The coarse size of the pumice clasts suggests the eruption involved either spalling from a shallow subaqueous dome (cf. Allen and McPhie 2000) or a proximal explosive eruption or a combination of the two. The lack of strong deformation of vesicles and of the contacts between the basaltic andesite and rhyolite implies little shear in the conduit and hence, low acceleration. This inference is consistent with the lack in most places of any fall deposits beneath unit A of the KPT (Allen 1998). The similarity in composition between the KPT and the Akra Chelona pumice suggests that similar magmas were involved in the two eruptions and thus the source vents likely had similar locations.

Pumice rafts and a beach deposit imply the presence of a body of water between Akra Chelona and the source vent for the pumice. Seismic reflection profiles show either lacustrine or marine sediments accumulated in a body of open water in the basin southeast of Kos and between the Datça and Bodrum peninsulas (Pe-Piper et al. 2005). At Akra Chelona at the time of the KPT eruption, the maximum fetch to the ENE was 40–50 km (Fig. 1a). The seismic reflection profiles suggest that the paleoshoreline paralleled the present southern coast of Kos east of Akra Chelona, but then turned southward towards Strongili (Fig. 1a). Seismic data density and younger faults make it impossible to precisely define where the coastline was located at the time of the KPT eruption. Elsewhere on Kos, the KPT overlies a paleosol or swamp horizon, or in places on the northern coast it overlies coastal dunes (Allen 1998). The paleo-sea-level compilation of Rabineau et al. (2006) suggests that eustatic sea level was at about −80 m and gradually falling at the time of the KPT eruption.

The regional seismic reflection data also suggest that the areas between the inferred KPT volcano and southwestern Kos, Tilos and Datça were dry land (Fig. 1a; Pe-Piper et al. 2005). Any evidence in the area of the source volcano was of course destroyed by the KPT eruption and further masked by younger volcanism. It would take only a narrow passage, such as the 1.5-km-wide passage at Santorini prior to the Minoan eruption (Druitt and Francaviglia 1992), to allow access of sea or lake water to the KPT vent to facilitate the main phreatomagmatic eruption (Allen and Cas 1998) and to link the basin east of Akra Chelona to the open sea to the southwest (Fig. 1a).

## The nature of the mafic and felsic magmas

The Mg-rich forsterite ($Fo_{89}$) and Ca-rich bytownite ($An_{87}$) phenocrysts in the more mafic basaltic andesite (CS167) suggest crystallisation in a parent mafic magma derived from mantle peridotite. The differences in phenocryst composition between the less (CS166) and more (CS167) mafic basaltic andesite pebbles imply basalt fractionation in a base-of-crust magma chamber as inferred by Wyers and Barton (1989) and subsequent authors (Bachmann et al. 2007, Pe-Piper and Moulton 2008), yielding basaltic andesite eruptive products.

The strongly lobate contacts and chilling of the mafic magma against the rhyolite, indicate that basaltic andesite and rhyolite (perhaps a crystal mush) co-existed as immiscible magmas. Nevertheless, the small rhyolite enclaves in the basaltic andesite suggest that some complete assimilation took place. The less mafic basaltic andesite sample (CS166), together with a glassy andesitic enclave in a rhyolite clast from unit E of the KPT (Pe-Piper and Moulton 2008), have compositions that could result from mixing of basaltic andesite CS167 with rhyolitic pumice (Fig. 5). In contrast, the andesitic lithic clasts in unit E of the KPT have lower concentrations of compatible elements such as Mg and Cr (Fig. 5a, c), comparable with post-KPT andesites erupted on Nisyros (Vanderkluysen et al. 2005), interpreted as resulting from continuing base-of-crust fractionation. Rhyolite erupted during the KPT shows only slight compositional changes with stratigraphic level; higher rhyolites are more siliceous and have higher $\varepsilon_{Nd}$. The elemental and isotopic composition of the rhyolite pumice cobbles is consistent with the trends inferred for a zoned magma chamber.

In summary, the basaltic andesite pebbles from the beach deposit at Akra Chelona represent the most primitive mafic magma known from the Quaternary Kos–Nisyros volcanic system, previously known only from a lithic clast in the

post-KPT Stavros pyroclastics on Nisyros. Less primitive basaltic andesite and the andesitic glass found in unit E of the KPT were partly the result of fractionation in a base-of-crust magma chamber and partly the result of mixing with rhyolite.

### Implications for post-KPT neotectonics

The KPT eruption at 161 ka took place when global eustatic sea level was about 80 m below its present level (Rabineau et al. 2006). The Akra Chelona beach deposit is now 49 m above sea level, implying ~120 m of neotectonic uplift over 161 ka, or ~0.75 mm/a. This rate compares with mean neotectonic subsidence rates as great as 3 mm/a in the West Kos basin south of Akra Chelona, determined from the depth of the unconformity created by the Marine Isotope Stage 6–5 transgression, which now lies several hundred metres below sea level (Fig. 11 of Pe-Piper et al. 2005).

Several other lines of evidence indicate post-KPT neotectonic activity on Kos. Faults cut the KPT in the western part of the Kefalos Peninsula (Ebner and Grasemann, 2007). Terraces geomorphologically resembling raised marine terraces are found in Kefalos Bay in the west and at Agios Fokas in the east (Fig. 1a). East of Kos town, at least two terraces are capped by shallow marine sediments of the Nicholaos Formation (Böger et al. 1974) of middle Pleistocene age (Desio 1931). Geomorphologically fresh fault scarps cut the Dikeos massif in southeastern Kos. Overall, the southern part of the island of Kos appears to have risen in the late Pleistocene, while the marine basins to the south and west have subsided. The beach deposit at Akra Chelona is the best dated reference point on land for such neotectonic uplift.

## Conclusions

1. A conglomerate of pumice cobbles and basaltic andesite pebbles immediately beneath the KPT at Akra Chelona is a beach deposit. The pumice cobbles probably accumulated where a pumice raft was stranded at the coast. The pumice closely resembles pumice from unit A of the KPT in composition and petrography and differs from rhyolites on the Kefalos Peninsula.
2. The presence of the beach deposit composed of rafted pumice is consistent with previous interpretations of ready access of water to the early phases of the KPT eruption (Allen and Cas 1998) and of a paleoshoreline in the vicinity of Akra Chelona (Pe-Piper et al. 2005).
3. The beach deposit implies a mean uplift rate of ~0.75 mm/a since the KPT eruption. Southern Kos has been uplifted many tens of metres and the marine areas to the south have subsided a few hundreds of metres since the KPT eruption, as a result of regional neotectonics.
4. The rhyolitic pumice contains numerous pebble-sized enclaves of basaltic andesite. The textures suggest the co-existence of mafic and felsic magma. This basaltic andesite may have triggered the KPT eruption. In its compatible element content and phenocryst composition, it is the most primitive eruptive product of the Kos–Nisyros volcanic system. Variation in composition of the basaltic andesite and of andesite erupted as part of the KPT indicates fractionation in a base-of-crust magma chamber was followed by assimilation of rhyolite during eruption.
5. The precursory activity produced rhyolite pumice rafts with basaltic andesite enclaves. A low eruption rate at this stage may have minimised the effects of mixing, so the two magma types were preserved.

**Acknowledgements** Field and laboratory work were supported by a Natural Sciences and Engineering Research Council of Canada discovery grant to GPP. We thank P. S. Giles and M. Salisbury for internal review and journal reviewers Claudia Principe and particularly Sharon Allen and associate editor Jocelyn McPhie for constructive criticism and advice. Geological Survey of Canada contribution 20090136.

## References

Allen SR (1998) Volcanology of the Kos Plateau Tuff, Greece: the product of an explosive eruption in an archipelago. PhD thesis, Monash University, Australia

Allen SR (2001) Reconstruction of a major caldera-forming eruption from pyroclastic deposit characteristics: Kos Plateau Tuff, eastern Aegean Sea. J Volcanol Geotherm Res 105:141–162

Allen SR, Cas RAF (1998) Rhyolitic fallout and pyroclastic density current deposits from a phreatoplinian eruption in the eastern Aegean Sea. J Volcanol Geotherm Res 86:219–251

Allen SR, Cas RAF (2001) Transport of pyroclastic flows across the sea during the explosive, rhyolitic eruption of the Kos Plateau Tuff, Greece. Bull Volcanol 62:441–456

Allen SR, McPhie J (2000) Water-settling and resedimentation of submarine rhyolitic pumice at Yali, eastern Aegean, Greece. J Volcanol Geotherm Res 95:285–307

Allen SR, Stadlbauer E, Keller J (1999) Stratigraphy of the Kos Plateau Tuff: product of a major Quaternary rhyolitic eruption in the eastern Aegean, Greece. Int J Earth Sci 88:132–156

Allen SR, Vougiokalakis GE, Schnyder C, Bachmann O, Dalabakis P (2009) Comments on: On magma fragmentation by conduit shear stress: Evidence from the Kos Plateau Tuff, Aegean Volcanic Arc, by Palladino, Simei and Kyriakopoulos (JVGR (2008) 178, 807–817). J Volcanol Geotherm Res 184:487–490

Bachmann O, Charlier BLA, Lowenstern JB (2007) Zircon crystallization and recycling in the magma chamber of the rhyolitic Kos Plateau Tuff (Aegean arc). Geology 35:73–76

Bluck BJ (1999) Clast assembling, bed-forms and structure in gravel beaches. Trans Roy Soc Edin Earth Sci 89:291–323

Böger H, Gersonde R, Willmann R (1974) Das Neogen in Osten der Insel Kos (Ägäis, Dodekanes)—Stratigraphie und tektonik. N Jb Geol Paläontol Abh 145:129–152

Bouvet de Maisonneuve C, Bachmann O, Burgisser A (2009) Characterization of juvenile pyroclasts from the Kos Plateau Tuff (Aegean Arc): insights into the eruptive dynamics of a large rhyolitic eruption. Bull Volcanol 71:643–658

Bryan SE, Cook A, Evans JP, Colls PW, Wells MG, Lawrence MG, Jell JS, Greig A, Leslie R (2004) Pumice rafting and faunal dispersion during 2001–2002 in the Southwest Pacific: record of a dacitic submarine explosive eruption from Tonga. Earth Planet Sci Lett 227:135–154

Desio A (1931) Le isole italiane dell'Ego. Mem descr carta geol Ital 24:1–547

Druitt TH, Francaviglia V (1992) Caldera formation on Santorini and the physiography of the islands in the late Bronze age. Bull Volcanol 54:484–493

Ebner M, Grasemann B (2007) Pliocene-Pleistocene tectonics in the Dodecanese (W-Kos, Greece). Geophys Res Abstr 9:131

Fujino S, Masuda F, Tagomori S, Matsumoto D (2006) Structure and depositional processes of a gravelly tsunami deposit in a shallow marine setting: Lower Cretaceous Miyako Group, Japan. Sed Geol 187:127–138

Heiken GH, McCoy FW (1990) Precursory activity to the Minoan eruption, Thera, Greece. In: Hardy DA, Renfrew AC (eds) Thera and the Aegean World III. The Thera Foundation, London 2, pp 79–88

Morton RA, Gelfenbaum G, Jaffe BE (2007) Physical criteria for distinguishing sandy tsunami and storm deposits using modern examples. Sed Geol 200:184–207

Murphy MD, Sparks RS, Barclay J, Carroll MR, Bewer TS (2000) Remobilization of andesite magma by intrusion of mafic magma at the Soufriere Hills volcano, Montserrat, West Indies. J Petrol 41:21–42

Pe-Piper G, Piper DJW (2002) The igneous rocks of Greece. Gebrüder Borntraeger, Berlin

Pe-Piper G, Piper DJW (2005) The South Aegean active volcanic arc: relationships between magmatism and tectonics. Devel Volcanol 7:113–133

Pe-Piper G, Moulton B (2008) Magma evolution in the Pliocene–Pleistocene succession of Kos, South Aegean arc (Greece). Lithos 106:110–124

Pe-Piper G, Piper DJW, Perissoratis C (2005) Neotectonics and the Kos Plateau Tuff eruption of 161 ka, South Aegean arc. J Volcanol Geotherm Res 139:315–338

Rabineau M, Berné S, Olivet J-L, Aslanian D, Guillocheau F, Joseph P (2006) Paleo sea levels reconsidered from direct observation of paleoshoreline position during Glacial Maxima (for the last 500, 000 yr). Earth Planet Sci Lett 252:119–137

Shane P, Nairn IA, Smith VC (2005) Magma mingling in the similar to 50 ka Rotoiti eruption from Okataina Volcanic Centre: implications for geochemical diversity and chronology of large volume rhyolites. J Volcanol Geotherm Res 139: 295–313

Simkin T, Fiske RS (1983) Krakatau 1883: the volcanic eruption and its effects. Smithsonian Institution, Washington DC

Stadlbauer E (1988) Volkanologische-geochemische Analyse eines jungen Ignimbrites: Der Kos-Plateau-Tuff (Südost-Ägäis). PhD thesis, Freiburg, Germany

Vanderkluysen L, Volentik A, Hernandez J, Hunzicker JC, Bussy F, Principe C (2005) The petrology and geochemistry of lavas and tephras of Nisyros Volcano (Greece). Mem Géol Lausanne 44:79–99

Willmann R (1983) Neogen und jungtertiäre Entwicklung der Insel Kos (Ägäis, Griechenland). Geol Rund 72:815–860

Wyers GP, Barton M (1989) Polybaric evolution of calc-alkaline magmas from Nisyros, southeastern Hellenic Arc, Greece. J Petrol 30:1–37